Acidic properties of sulfated iron oxide supported molybdenum catalysts: a differential scanning calorimetry, thermogravimetry and Fourier transform-infrared study

Mohamed Mokhtar Mohamed[a,*], Bahaa M. Abu-Zied[b]

[a]*Chemistry Department, Faculty of Science, Benha University, Benha, Egypt*
[b]*Chemistry Department, Faculty of Science, Assiut University, Assiut 71516, Egypt*

Abstract

Sulfated Fe_2O_3 catalysts impregnated with different molybdenum contents varied from 2 to 42 wt.%, were examined by temperature-programmed pyridine desorption via differential scanning calorimetry (DSC) and thermogravimetry (TG) techniques. The acidity of these catalysts were investigated and compared with those corresponding to SO_4^{2-}/free Fe_2O_3 ones. ΔH values (obtained from DSC) and amounts of pyridine irreversibly adsorbed (obtained from TG) showed that the concentration of Lewis acid sites decreased with increasing Mo loading. On the other hand, the sulfated Fe_2O_3 supported Mo catalysts showed an increase in the concentration of acid sites to almost 10 times that of the corresponding SO_4^{2-}/free Fe_2O_3 catalysts. In addition, the enthalpies of pyridine desorption from SO_4^{2-}/Fe_2O_3 supported Mo catalysts were higher than those for the SO_4^{2-}/free Fe_2O_3 catalysts. This indicated the strength of acid sites on the former samples compared with those on the later ones. Comparative FT-IR spectroscopic analyses of pyridine adsorption have been investigated to study the nature of the acid sites and to assess the effect of SO_4^{2-} species on the surface acidity. It was found that the presence of SO_4^{2-} species enhanced the surface acidity and helped the formation of Brønsted sites earlier at the 2 wt.% Mo loading. These were manifested by the presence of vibrational bands at 1635 and 1540 cm^{-1}. These bands were only detected at a loading of 5 wt.% Mo when the support was SO_4^{2-}/free Fe_2O_3. Important correlations and shifts in the IR absorption bands were evaluated and discussed. © 2000 Elsevier Science B.V. All rights reserved.

Keywords: Acidity evaluation; MoO_3/SO_4^{2-}/Fe_2O_3 catalysts; DSC; TG; FT-IR

1. Introduction

There has been renewed interest in supported molydena catalysts because of their numerous applications in petroleum refining, chemicals production and pollution control [1–3]. Most of the studies have focused on silica supported molybdenum catalysts, usually prepared by impregnation using aqueous solutions of ammonium molybdate [4,5]. Supports other than silica, e.g. titania, zirconia, carbon or iron have received less attention [6–8].

Iron is the preferred support for molybdenum-based catalysts for conversion of coal to liquid fuel via direct coal liquefaction (DCL) [9]. Efforts have been devoted to produce high conversion rate of DCL. This has been achieved by sulfating the iron oxide catalyst (Fe_2O_3/SO_4^{2-}) as well as by adding small amounts of either

* Corresponding author.

Mo or W (Mo or W/Fe_2O_3/SO_4^{2-}) [10,11]. The role of SO_4^{2-} is to induce the formation of coordination-unsaturated sites (CUS), or Lewis acid sites, at the catalyst surface, and thereby increase the acidity of the catalysts [12,13]. The presence of SO_4^{2-} at the catalyst surface also inhibited the crystal growth of the Fe_2O_3 phase. Previous works [14,15] found that Fe was highly dispersed with an average diameter of 30 Å and the identified phase was FeOOH. A considerable amount of surface iron ions were found to be at CUS.

The DCL conversion was found to decrease if the catalyst was exposed to moist air before reaction because of the quick agglomeration and transformation of FeOOH to α-Fe_2O_3 that results in a significant reduction in surface area [16]. On the other hand, the presence of impurity ions (such as Mo or W) in the precipitation solution lead to preferential occupation on the CUS sites by such ions instead of water molecules and thereby crystal growth inhibition was achieved.

The aim of the present study is to characterize the acidic properties of sulfated iron oxide supported Mo catalysts with reference to the corresponding non-sulfated ones by means of TG, DSC and FT-IR techniques. These techniques enable us to determine the nature of the different acid sites exposed on the catalyst surface, as determined by FT-IR spectroscopy and to quantify these from the amount of pyridine adsorbed determined by TG, as well as measuring their strength from the enthalpies of desorption by DSC.

2. Experimental

2.1. Materials

The unsupported iron oxide samples were prepared by precipitation from an aqueous ferric nitrate solution [$Fe(NO_3)_3 \cdot 9H_2O$] with ammonium hydroxide. The pH was maintained between 10 and 10.5. The precipitate was washed repeatedly with water followed by removal of the supernatant liquid by decanting until pH=7. The solution was filtered, the cake precipitate was dried at 110°C for 4 h, to give FeOOH as determined by XRD analysis. Portions of the sample were ground to a fine powder, and calcined at 500°C in air for 6 h. The solid after calcination was α-Fe_2O_3.

The sulfur-promoted iron oxide was prepared by immersing the FeOOH in a solution of $(NH_4)_2SO_4$. The suspension was stirred for 1 h at room temperature, filtered on a Pyrex frit, and evaporated to dryness at 110°C for 10 h. Portions of the sample were calcined in air at 500°C for 6 h. The amount of $(NH_4)_2SO_4$ added was adjusted to yield iron oxide containing 5 wt.% of SO_4^{2-} ion.

The FeOOH sample (sulfated; SO_4^{2-}/FeOOH and non-sulfated FeOOH) were loaded with different weight percents of Mo by an impregnation technique. A 2.00 g of the sample were stirred in 50 cm^3 of an aqueous solution of ammonium heptamolybdate, $(NH_4)_6Mo_7O_{24} \cdot 4H_2O$, of the appropriate concentration to give samples loaded with 2, 5, 10 and 42 wt.% of molybdenum. The Mo loaded solids were dried without washing at 120°C for 6 h, and then calcined at 500°C in air for 6 h.

The FeOOH was used as the starting support during the preparations, due to its thermal transformation as that of molybdate into molybdena, in order to enhance the chance of solid–solid interactions. This was not possible to obtain upon using α-Fe_2O_3 as the starting support.

2.2. Pyridine adsorption

Portions of all the samples were transformed from the drying desiccator into another desiccator containing liquid pyridine. The transfer was carried out quickly to minimize the contact time with the ambient atmosphere. The samples were maintained in contact with pyridine vapor, at room temperature, for 1 month, prior to analysis.

2.3. Techniques

Pyridine coated samples ($\pm$10.0 mg) were subjected to TG analysis over the temperature range from ambient to 600°C at a heating rate of 10°C min^{-1} under dry air (40 cm^3 min^{-1}). The TG curves were automatically recorded on a model 2000 TA unit. The weight loss was measured as well as the derivative weight loss as a function of temperature. This was used to determine the amounts of pyridine irreversibly adsorbed. More details can be seen elsewhere [17].

The enthalpy change (ΔH) on pyridine desorption over a given temperature range was derived from a

power compensated DSC. DSC analyses of the samples were carried out using TA 2000. A 10 mg solid portion was used for the measurement. The rate of heating was $10°C\ min^{-1}$ and the measurements were carried out in flowing dry air at $40\ cm^3\ min^{-1}$.

Investigation of the nature of the acid sites (Lewis and Brønsted) was carried out using FT-IR spectroscopy using a Nicolet 710 spectrometer with pyridine adsorbed on the samples. Nominal resolution was $4\ cm^{-1}$, and 32 runs were averaged to improve the signal to noise ratio. The bands due to adsorbed pyridine were assigned to different modes following the data corresponding to liquid pyridine and protonated pyridine [18].

The X-ray powder diffraction of some calcined samples was measured using a Philips PW 213/00, using nickel-filtered Cu Kα radiation (λ=1.5405 Å) at 35 kV and 20 mA at a scanning rate of $2\theta=2°\ min^{-1}$.

3. Results and discussion

3.1. Desorption of presorbed pyridine from x wt.% MoO_3/Fe_2O_3 samples as measured by DSC

The DSC analyses shown in Fig. 1a–c exhibited two distinct desorption peaks from the parent Fe_2O_3

sample and after loading with 2 and 5 wt.% Mo, respectively. However, with the 42 wt.% Mo loading (spectrum d), three distinct exotherms were observed with an exotherm at high temperature region. DSC can easily differentiate between physically and chemically adsorbed phases through the thermogram as endothermic and exothermic transition peaks, respectively [19]. Moreover, DSC can measure the enthalpies of desorption which are proportional to the number of acid sites. Thus, the first endotherm in the former samples (a–c) represents the desorption of physisorbed pyridine (25–170°C), whereas the second exotherm represents the chemisorbed one (270–535°C) [19]. The small peaks in the DSC response of the d sample were not seen in samples a–c. Ascribing these peaks to physisorbed pyridine is likely, although of their high temperature range that extended from 25 to 280°C, because of the low amounts of pyridine adsorbed and the low values of enthalpies of desorption, as can be seen in Table 1. This table shows quantitative pyridine amounts and ΔH values obtained from pyridine desorption from the samples.

The second exotherm is asymmetric and is attributed to pyridine desorption from Lewis acid sites, since the sample is heated to 500°C to prevent the formation of proton-donor sites from water molecules

Table 1
Quantitative pyridine amounts and ΔH values obtained for TG and DSC effects, respectively, via pyridine desorption from the samples studied

Catalyst	Pyridine (ads. mmol g^{-1})	Temperature range (°C)	Peak maximum (°C)	Pyridine physical (ΔH, kJ mol^{-1})	Temperature range (°C)	Peak maximum (°C)	Pyridine chemical (ΔH kJ mol^{-1})
Fe_2O_3	0.06	25–125	78.9	3.0	220–470	332	9.6
2 wt.% Mo/Fe_2O_3	0.138	25–170	93.5	4.7	180–500	372.9	22.5
5 wt.% Mo/Fe_2O_3	0.106	25–170	84.7	4.2	270–535	400.9	17.9
42 wt.% Mo/Fe_2O_3	0.05	106–143	126.4	0.20	320–510	405.0	5.0
		147–183	153.2	0.23			
		210–280	224.0	0.57			
Fe_2O_3/SO_4^{2-}	0.11	25–97	61.2	0.46	315–510	382	7.6
		145–273	195.6	0.28			
2 wt.% Mo/Fe_2O_3/SO_4	1.31	30–170	99.6	4.8	280–510	401.2	23.0
5 wt.% Mo/Fe_2O_3/SO_4	1.25	25–245	98.8	7.6	290–501	402.7	19.8
10 wt.% Mo/Fe_2O_3/SO_4	1.14	25–115	69.2	1.33	280–470	400.2	19.5
42 wt.% Mo/Fe_2O_3/SO_4	0.56	30–80	61.9	0.47	295–507	394.8	11.6
SO_4		104–140	120.7	0.32			
		145–187	174	0.40			
		189–240	221	1.2			
		248–287	270	1.1			

Fig. 1. DSC thermograms of pyridine desorption from: (a) α-Fe$_2$O$_3$; (b) 2 wt.% Mo/Fe$_2$O$_3$; (c) 5 wt.% Mo/Fe$_2$O$_3$; and (d) 42 wt.% Mo/Fe$_2$O$_3$.

($Fe^{3+} \leftarrow OH_2$). It is known that only Lewis acid sites were formed on the iron oxide surface [20]. With increasing Mo wt.%, a gradual increase in the Lewis acid strength was noted as manifested by the shift in the exotherm temperature to higher values. A shift from 322°C in the parent sample to 405°C in the 42 wt.% Mo/Fe$_2$O$_3$ sample was recognized (Table 1). Contrarily, the amount of the Lewis acid sites was reduced on increasing the Mo loading from 2 to 42 wt.%. This decrease in the number of Lewis acid sites that associated with the high Mo loading was consistent with the change in ΔH values and the amounts of pyridine adsorbed (Table 1).

The enthalpies of desorption, ΔH, are considered to show the relative strengths of the acid sites involved. In the case of α-Fe$_2$O$_3$, the ΔH value for the endotherm was 3.0 kJ mol^{-1} [19]. On increasing the Mo loading from 2 to 5 wt.%, the enthalpies of desorption showed relatively higher values of 4.7 and 4.2 kJ mol^{-1}, respectively. On the other hand, the ΔH of desorption of the Lewis acid-pyridine from the α-Fe$_2$O$_3$ sample was 9.6 kJ mol^{-1}; a value that was consistent with a relatively stronger bonding to the pyridine. A systematic decrease in ΔH values was found from 2 to 42 wt.% Mo, indicating a decrease in the strength of the Lewis sites. This decrease in ΔH values parallels a decrease

in the temperature range of the respective peaks, also indicating a decrease in the strength of Lewis sites after 2 wt.% Mo loading. It seems that iron substrate stabilizes Mo cations in the sites of low coordination, thereby leading to the formation of stronger acid sites [21], as can be seen for 2 and 5 wt.% Mo samples.

The significant decrease in the strength of the Lewis acid sites with increasing Mo loading was also confirmed from changes in the IR spectra on pyridine adsorption, as depicted in Fig. 2. This figure shows the IR spectra of adsorbed pyridine on Mo-free Fe_2O_3 support and after loading with 2, 5 and 42 wt.% Mo designated as a, b, c and d, respectively. A shift to lower frequency was observed for the Lewis bands from 1632 to 1618 and 1452 to 1446 cm^{-1}, indicating the weakening of the bonding to these sites. A parallel increase in Brønsted acid sites was indicated by the appearance of a band at 1635 cm^{-1} and a shoulder at 1541 cm^{-1} (spectrum c), which supports the presence of pyridinium ion. The amounts of pyridine adsorbed, which indicate the concentration of adsorption sites, were consistent with the change in ΔH values. The amounts of pyridine irreversibly adsorbed on the α-Fe_2O_3 sample (0.06 mmol g^{-1}) were almost similar to that measured by Tanabe and co-workers (0.052 mmol g^{-1}) [20].

The decrease in the number of acid sites shown by the amount of pyridine adsorbed for the high Mo loading (42 wt.%) as well as the significant decrease in ΔH values is due to the reaction of the Fe_2O_3 oxide with molybdate species to form the corresponding iron-molybdates. The presence of iron-molybdate was only found in the 42 wt.% Mo sample, as detected by X-ray measurements (not shown). The dramatic decrease in the number of acid sites, especially those of Lewis acid sites, is dependent on the production of $Fe_2(MoO_4)_3$. This has a dramatic effect in reducing the concentration of polymolybdate species, which has a high acidity.

An increase in the Bpy/Lpy ratio as the Mo loading increases to 42 wt.% can also be seen in Table 2. This showed the changes in the positions of the FT-IR absorption bands due to vibrational modes of pyridine (19b and 8a) and the areas of the bands due to the 19b mode of Bpy and Lpy sites at 1537–1541 and 1445–1452 cm^{-1}, respectively, together with their ratio (Bpy/Lpy). Consequently, the presence of Brønsted
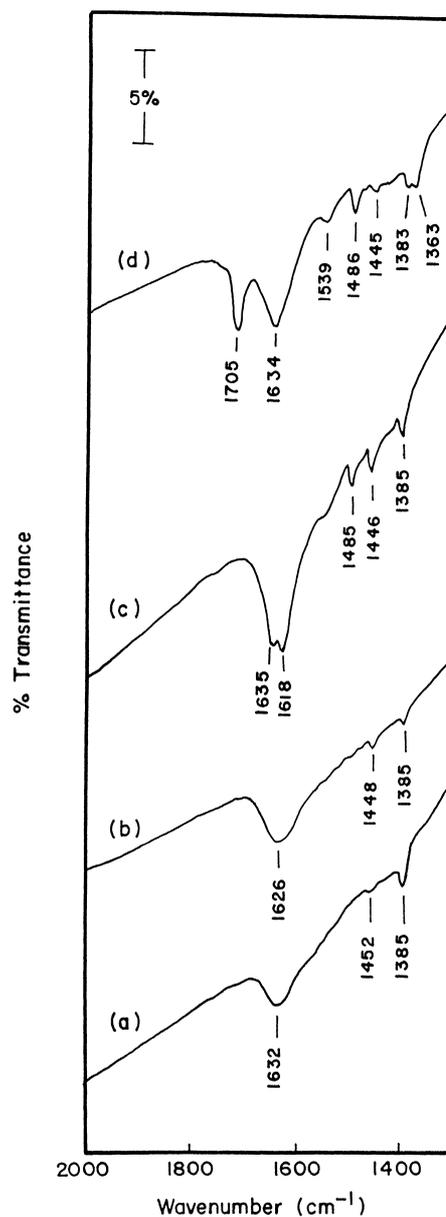
Fig. 2. FT-IR spectra recorded after pyridine adsorption at room temperature, in the 2000–1300 cm^{-1} range, on the following catalysts supported on α-Fe_2O_3: (a) parent α-Fe_2O_3; (b) 2 wt.% Mo; (c) 5 wt.% Mo; and (d) 42 wt.% Mo.

acidity, when the Mo/Fe ratio increases, indicates that the exotherm, occurred in the high temperature region, in Fig. 1 represents not only Lewis but also Brønsted acidity.

Table 2
FT-IR absorption bands (cm^{-1}) for normal modes of pyridine, recorded upon adsorption at room temperature on the samples studied

Sample	Bby		Lpy		Bpy/Lpy
	8a	19b	8a	19b	
Fe_2O_3	–	–	1632	1452	–
2 wt.% Mo/Fe_2O_3	–	–	1626	1448	–
5 wt.% Mo/Fe_2O_3	1635	1541	1618	1446	0.23
42 wt.% Mo/Fe_2O_3	1634	1539	–	1445	1.5
Fe_2O_3/SO_4^{2-}	–	–	1632	–	–
2 wt.% $Mo/Fe_2O_3/SO_4^{2-}$	1635	1538	1621	–	–
5 wt.% $Mo/Fe_2O_3/SO_4^{2-}$	1633	1540	–	–	–
10 wt.% $Mo/Fe_2O_3/SO_4^{2-}$	1630	1538	–	1446	2.0
42 wt.% $Mo/Fe_2O_3/SO_4^{2-}$	1633	1539	–	1444	1.0

3.2. Desorption of presorbed pyridine from x wt.% $MoO_3/Fe_2O_3/SO_4^{2-}$ samples as measured by DSC

Fig. 3 shows the DSC response (a) of pyridine desorption from the unloaded Fe_2O_3/SO_4^{2-} and after loading with 2, 5, 10 and 42 wt.% Mo samples (b–e). Sulfated iron exhibited one small endotherm with maximum rate of heat evolution at 61.2°C and an exotherm at 382°C. Comparing these with those obtained from the Fe_2O_3 sample, an increase in acid sites concentration was found and confirmed by enhancing the amounts of pyridine adsorbed to 0.11 mmol g^{-1} for Fe_2O_3/SO_4^{2-} compared to 0.06 mmol g^{-1} for the Fe_2O_3 sample (Table 1). A shift of the exotherm peak temperature from 322°C in the Fe_2O_3 sample to 382°C in the Fe_2O_3/SO_4^{2-} sample was also detected (Table 1). This is due to the weakening of the S=O bonds, induced by electron transfer from the pyridine molecules (strong base) to the Fe^{3+} cation (Lewis acid site) [7] or by direct interaction of the pyridine molecule with sulfated species.

The infrared spectra of the unloaded Fe_2O_3/SO_4^{2-} sample and after loading with 2, 5, 10 and 42 wt.% Mo are designated a, b, c, d and e, respectively, are shown in Fig. 4. These spectra confirmed the increasing amounts of pyridine adsorbed from the increase in the intensity of the Lewis band at 1632 cm^{-1} for the Fe_2O_3/SO_4^{2-} sample (spectrum a) compared with the corresponding analogue in the Fe_2O_3 sample (Fig. 2a). The former spectrum (4a) also confirmed the absence of Brønsted sites as detected by others for sulfated zirconia [22].

Increasing the Mo loading on the Fe_2O_3/SO_4^{2-} sample showed a remarkable increase in the amounts of pyridine adsorbed, as shown in Table 1. This indicates the increase in the number of acid sites. As can be seen in Table 1, the amounts of pyridine adsorbed over 2, 5 and 42 wt.% $Mo/Fe_2O_3/SO_4^{2-}$ showed an enhancement of almost 10 times to that of the corresponding non-sulfated samples. This was associated with a small little shift in the peak maximum (401–394°C), indicated for the x wt.% $MoO_3/Fe_2O_3/SO_4^{2-}$ samples, and reflected the high stability of acid strength of these samples. In addition, the enthalpies of desorption, ΔH, of the Mo loaded F_2O_3/SO_4^{2-} samples, in the high temperature range, were higher than the corresponding analogies on Fe_2O_3. This may account for the marked enhancement of the electron deficiency on Fe^{3+} that has been obtained by the introduction of both sulfate and Mo ions. This is explained by the high Sanderson electronegativity of the latter ions compared with the former one that enhances the unsaturation of the Fe ions for the easier attack by pyridine molecule. The remarkable enhancement in the amounts of pyridine adsorbed on sulfated iron oxide supported Mo catalysts was also revealed from the spectroscopic results that showed a marked increase in the concentration of the Brønsted sites. The increase in these sites can be seen in Table 2 that showed the highest Bpy/Lpy ratio at the 10 wt.% Mo loading.

The pyridine desorption measured by DSC for the 42 wt.% $Mo/Fe_2O_3/SO_4^{2-}$ sample (thermogram 3e and Table 1) showed two extra endotherms with maximum at 61.9 and 270°C compared with the
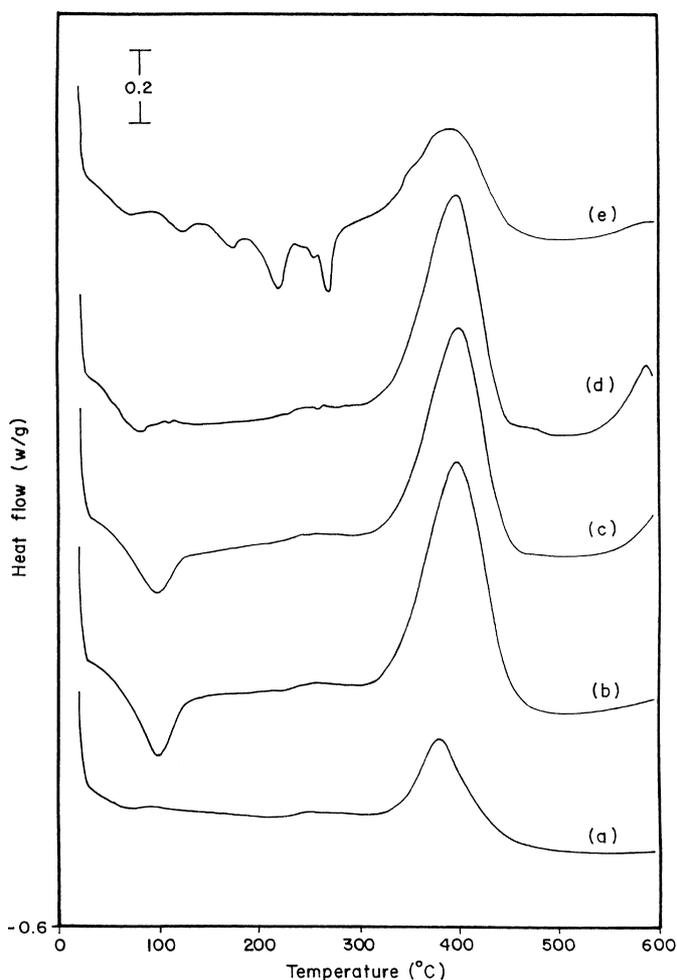
Fig. 3. DSC thermograms of pyridine desorption from: (a) SO_4^{2-}/Fe_2O_3; (b) 2 wt.% $Mo/Fe_2O_3/SO_4^{2-}$; (c) 5 wt.% $Mo/Fe_2O_3/SO_4^{2-}$; (d) 10 wt.% $Mo/Fe_2O_3/SO_4^{2-}$; and (e) 42 wt.% $Mo/Fe_2O_3/SO_4^{2-}$.

corresponding 42 wt.% Mo/Fe_2O_3 sample, in the low temperature range. This can be explained in terms of the interaction between Mo and Fe_2O_3 that promote a modified acidic property and thereby leading to the formation of weak acid sites.

Interestingly, from the X-ray analysis data, the 42 wt.% $Mo/Fe_2O_3/SO_4^{2-}$ sample showed a decrease in intensity for $Fe_2(MoO_4)_3$ and MoO_3 phases compared with the corresponding analogue of the non-sulfated sample. This indicates the improved dispersion of these species in the sulfated sample. The presence of these phases was responsible for the acidity decrease on the sulfate free Fe_2O_3 supported

Mo catalysts, e.g. 0.56 mmol g^{-1} for the 42 wt.% $Mo/Fe_2O_3/SO_4^{2-}$ sample compared with 0.05 mmol g^{-1} for the 42 wt.% Mo/Fe_2O_3 one. This can be due to sulfate group that helps to expose more active Mo^{6+} sites to coordinate with pyridine molecules.

The concentration of Brønsted sites in both 2 and 5 wt.% Mo samples on sulfated Fe_2O_3 support was higher than those in sulfate free ones (Table 2). This is attributed to the presence of polymolybdate species (i.e. bridging M–O bond) and Mo−OH sites. A further increase in the Mo loading over the former support causes a marked decrease in the ratio, confirming diminishing of Brønsted sites. This is due to the
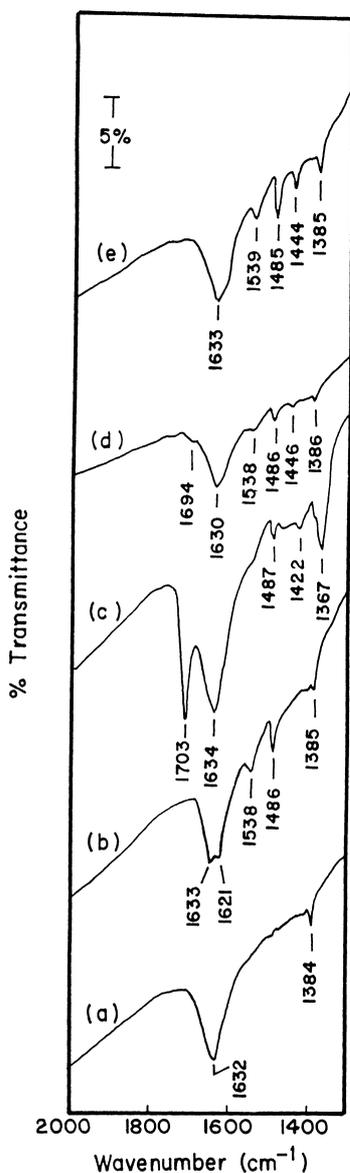
Fig. 4. FT-IR spectra recorded after pyridine adsorption at room temperature, in the 2000–1300 cm^{-1} range, on the following catalysts supported on SO_4^{2-}/Fe_2O_3: (a) parent SO_4^{2-}/Fe_2O_3; (b) 2 wt.% Mo; (c) 5 wt.% Mo; (d) 10 wt.% Mo; and (e) 42 wt.% Mo.

formation of iron-molybdate that destroyed the Brønsted sites. This decrease of surface Brønsted acid sites may partly related to the difference in electronegativity between Fe and Mo atoms (Mo ← O ← Fe) that leads to resume Lewis acidity.

4. Conclusions

The main conclusions that can be derived from the obtained results are as follows:

1. TG and DSC of the temperature programmed desorption of pyridine can provide quantitative information about the concentration and strength of acid sites exposed on a catalyst surface. ΔH values, pyridine concentrations, temperature ranges, and the temperature of the exotherm maxima were correlated well with the surface acidity. It was shown that sulfate group increased the amount of pyridine adsorbed on iron oxide loaded Mo to almost 10 times that of the non-sulfated catalysts. This enhanced acidity was also confirmed from the high ΔH values and the constancy of the exotherm peak maximum at the high temperature range.

2. IR spectra confirmed the presence of Brønsted overlapping with the Lewis acid sites in the exotherm peak as the Mo loading varied from 2 to 10 wt.%. Contrary, at high Mo loading (42 wt.%), a significant reduction in former site was developed. This decrease was due to cancellation of some Brønsted sites (Mo–OH) as a result of iron molybdate formation.

3. The high dispersion provided for Mo species on sulfated samples compared with sulfate free samples especially at high loading (42 wt.% Mo) was responsible for enhancing the acidity of sulfated iron supported Mo samples. This result was confirmed from ΔH values and amounts of pyridine adsorbed.

References

[1] R. Prins, V.H.J. De Beer, G.A. Somorjai, Catal. Rev. Sci. Eng. 31 (1989) 1.

[2] H. Knozinger, in: M.J. Phillips, M. Ternan (Eds.), Proceedings of the 9th International Congress on Catalysts, Vol. 5, Calgary, 1988, Chemical Institute of Canada, Ottawa, p. 20.

[3] K. Bruckman, B. Grzybowska, M. Che, J.M. Tatibouet, Appl. Catal. A: General 96 (1993) 279, and references therein.

[4] M.M. Mohamed, G.M.S. El Shafei, Spectrochim. Acta 51A (1995) 1525.

[5] G.M.S. El Shafei, M.M. Mohamed, Colloid Surf. 94A (1995) 267.

[6] C. Martin, I. Martin, C. Del Moral, V. Rives, J. Catal. 146 (1994) 415.

[7] F. Babou, G. Coudurier, J.C. Vedrine, J. Catal. 152 (1995) 341.

[8] K. Chem, Y. Fan, Z. Hu, Q. Yan, Catal. Lett. 36 (1996) 139.

[9] K. Tanabe, H. Hattori, T. Yamaguchi, T. Lizuka, H. Matzuhashi, Fuel Process. Technol. 14 (1986) 247.

[10] B.J. Liaw, D.S. Cheng, B.L. Yang, J. Catal. 118 (1989) 312.

[11] M. Farcasiu, unpublished results.

[12] V.R. Pradhan, J.W. Tierney, I. Wender, G.P. Huffman, Energy Fuels 5 (1991) 497.

[13] T. Jin, Y. Yamaguchi, K. Tanabe, J. Phys. Chem. 90 (1986) 4795.

[14] J. Zhao, F.E. Huggins, Z. Feng, F. Lu, N. Shah, G.P. Huffman, J. Catal. 143 (1993) 499.

[15] Z. Feng, J. Zhao, F.E. Huggins, G.P. Huffman, J. Catal. 143 (1993) 510.

[16] J. Zhao, Z. Feng, F.E. Huggins, N. Shah, G.P. Huffman, I. Wender, J. Catal. 148 (1994) 194.

[17] H.M. Ismail, S.A.A. Mansour, M.I. Zaki, Thermochim. Acta 202 (1992) 269.

[18] M.M. Mohamed, Spectrochim. Acta 51A (1995) 1.

[19] A. Aboul-Gheit, J. Catal. 113 (1988) 490.

[20] A. Kayo, T. Yamaguchi, K. Tanabe, J. Catal. 83 (1983) 99.

[21] J.R. Sohn, H.J. Kim, J. Mol. Catal. 52 (1989) 379.

[22] M. Bensitel, O. Saur, J.C. Lavalley, Mater. Chem. Phys. 17 (1987) 249.